

Label Hierarchy Transition: Delving into Class Hierarchies to Enhance Deep Classifiers

Renzhen Wang, De Cai, Kaiwen Xiao, Xixi Jia, Xiao Han, Deyu Meng, Member, IEEE

Abstract—Hierarchical classification aims to sort the object into a hierarchical structure of categories. For example, a bird can be categorized according to a three-level hierarchy of order, family, and species. Existing methods commonly address hierarchical classification by decoupling it into a series of multi-class classification tasks. However, such a multi-task learning strategy fails to fully exploit the correlation among various categories across different levels of the hierarchy. In this paper, we propose Label Hierarchy Transition (LHT), a unified probabilistic framework based on deep learning, to address the challenges of hierarchical classification. The LHT framework consists of a transition network and a confusion loss. The transition network focuses on explicitly learning the label hierarchy transition matrices, which has the potential to effectively encode the underlying correlations embedded within class hierarchies. The confusion loss encourages the classification network to learn correlations across different label hierarchies during training. The proposed framework can be readily adapted to any existing deep network with only minor modifications. We experiment with a series of public benchmark datasets for hierarchical classification problems, and the results demonstrate the superiority of our approach beyond current state-of-the-art methods. Furthermore, we extend our proposed LHT framework to the skin lesion diagnosis task and validate its great potential in computer-aided diagnosis. The code of our method is available at <https://github.com/renzhenwang/label-hierarchy-transition>.

Index Terms—Hierarchical classification, transition network, confusion loss, low-shot learning, computer-aided diagnosis.

1 INTRODUCTION

IMAGE classification is a classic computer vision task that aims to predict a category label for each image. Recent years have witnessed the tremendous success of image classification due to the rapid development of deep learning [1], especially for deep classification networks [2], [3], [4]. Conventionally, a classification network is trained with cross-entropy loss on one-hot labels, such that it predicts almost orthogonal category labels for images in different classes. Such a scheme focuses on the differences of categories, albeit it may encounter challenges in effectively capturing inter-class similarity [5], [6]. Hierarchical classification, contrast to classic image classification, attempts to classify the object into a hierarchy of categories, with each hierarchy represents one specific level of concept abstraction. For example, birds can be categorized into a three-level hierarchy of order, family and species according to their taxonomic characters, as shown in Fig. 1. In hierarchical classification learning, the labels can be organized according to the domain knowledge (e.g, WordNet database [7]) or automatically generated by algorithms [8], [9], [10], [11], [12]. Compared to traditional multi-class classification, hierarchical classification pays more attention to exploit rich semantic correlation among categories [13], in order to improve the performance





Hierarchy				
Species	YW	NW	RW	HW
Family	Par		Trog	
Order	Pass			

Fig. 1: Illustration of a representative hierarchical classification scenario, where a bird is classified within a hierarchical structure comprising three levels: *species*, *family*, and *order*. The objects within the same hierarchy commonly share rich semantic correlation. Abbreviations: Yellow Warbler (YW), Nashville Warbler (NW), Rock Wren (HW), Parulidae (Par), Troglodytidae (Trog), Passeriformes (Pass).

of traditional classification tasks [14], [15] or mitigate the severity of prediction mistakes [16], [17], i.e., making the incorrectly classified samples fall within semantically related categories. Take the example of making diagnosis for one malignant tumor, mistaking it as another malignant one in the same subtype should be much less serious than mistaking it as one benign tumor, as such a mistake would have crucial implications in terms of the follow-up diagnosis and treatment.

Hierarchical classification has been proved effective in many visual scenarios, which can be traced back to traditional linear classifiers [18], [19], [20], [21]. Recently, hierarchical classification has attracted much attention in deep learning [22]. Most of the existing works [16], [23], [24], [25], [26] commonly fall into a multi-task learning manner. For example, a deep network was proposed in [23] to classify coarse- and fine-level categories through two different branches. In [16], a granular network was proposed for food

- Renzhen Wang and Deyu Meng (corresponding author) with School of Mathematics and Statistics and Ministry of Education Key Lab of Intelligent Networks and Network Security, Xi'an Jiaotong University, Xi'an 710049, Shaanxi, P.R.China.
E-mail: {rzwang,dymeng}@xjtu.edu.cn
- De Cai, Kaiwen Xiao and Xiao Han are with Tencent AI Lab, Shenzhen 518057, Guangdong, P.R.China.
E-mail: caide199212@gmail.com; {loktarxiao,haroldhan}@tencent.com
- Xixi Jia with school of Mathematics and Statistics, Xidian University, Xi'an 710049, Shaanxi, P.R.China.
E-mail: hsiijiaxidian@gmail.com

image classification, where a single network backbone was shared by multiple fully-connected layers with each one responsible for the label prediction within one hierarchy. Chen et al. [25] likewise employed a multi-head architecture to level-wisely output the prediction, but instead introduced an attention mechanism to guide label prediction of fine-level hierarchy through that of the coarse-level hierarchy. Furthermore, Alsallakh et al. [24] used a standard deep architecture to fit the finest-level labels, and added branches at the intermediate layers to fit the coarser-level labels. All the above methods adopt a divide-and-conquer strategy to model the class hierarchies, in which the semantic correlation of labels are implicitly captured by the gradient back propagation of the multi-task loss, e.g., the sum of cross-entropy losses of each hierarchy. Recently, Chang et al. [26] pointed out that fine-level features benefit coarse-grained classifier learning, yet coarse-level label prediction is harmful to fine-level feature learning. They in turn proposed to disentangle coarse- and fine-level features by leveraging level-specific classification heads, and further force finer-grained features (with stopped gradient) to participate in coarser-level label predictions. Such a simple method has achieved significant improvement in fine-level image recognition, which, however, does not explicitly make use of the class hierarchies. Moreover, the cross-entropy loss with one-hot labels used in these existing methods incline to produce orthogonal predictions at each hierarchy and fail to depict the correlation among different categories.

The aim of this study is to develop a deep hierarchical classification method capable of explicitly capturing the semantic correlation embedded in class hierarchies. Inspired by the hierarchical labeling process of human [26] that an accurate annotation usually depends on the image itself and the label at the adjacent hierarchy, we propose Label Hierarchy Transition (LHT), a unified probabilistic approach, to recursively predict the labels from fine- to coarse-level class hierarchies. Concretely, the LHT model contains two components: (1) an arbitrary existing classification network, which is used to predict the labels for the finest-level hierarchy; (2) a transition network, which generates a label hierarchy transition matrix for each hierarchy (except for the finest-level one). Each element of the transition matrix denotes the conditional probability of one class at the corresponding hierarchy given the other class of the adjacent finer-level hierarchy. For each coarser-level hierarchy, the label prediction can be formulated as the product of its corresponding transition matrix and the prediction score of its adjacent finer-level hierarchy. To address the over-confident prediction problem introduced by the cross-entropy loss, we further propose a confusion loss that explicitly regularizes the label hierarchy transition matrices, and encourages the network to learn semantic correlation from all class hierarchies during training.

In summary, the main contributions are three-fold:

- We propose a unified deep classification framework to address the hierarchical classification problem. Contrast to predicting the labels for each hierarchy, we propose to learn label hierarchy transition matrices, which encode the likelihood of similarity between classes across different label hierarchies. To the best of our knowledge, we are the first to lever-

age deep networks to explicitly learn the semantic correlation embedded in class hierarchies.

- We propose a confusion loss to directly regularize the negative entropy of the column space of label hierarchy transition matrices, which further encourages the network to learn correlations among class hierarchies, and alleviates the issue of overconfident predictions arising from cross-entropy loss.
- Our LHT method can be readily applied to any existing classification network, and the resulting model can be trained in an end-to-end manner. Extensive experiments on a series of hierarchical classification tasks demonstrate the superiority of our approach beyond the prior arts.

The rest of this paper is organized as follows. Section 2 revisits related work. Section 3 describes the formulation of the proposed LHT framework as well as its training algorithm. Section 4 presents experimental results and analysis in detail. Section 5 provides a realistic application of our method in computer-aided diagnosis. Section 6 summarizes the final conclusion.

2 RELATED WORK

Hierarchical classification [27], [28], [29], exploiting a hierarchical structure of labels for classification task, has been extensively explored in natural language processing [30], [31], [32], computer vision and computer-aided diagnosis [33], [34], [35]. In the existing literatures, hierarchical classification is mainly related to three aspects of research: hierarchical architecture, hierarchical loss function and label embedding based methods. Next we discuss related studies with respect to these three aspects.

2.1 Hierarchical architecture

A common way of designing a hierarchical architecture is to alleviate the computational burden of traditional linear classifiers when the number of recognition categories become huge [21], [36], [37], [38], [39]. The core idea was to create a tree-like classifier whose leaf nodes were used for the prediction of the given categories and internal nodes for the cluster of categories.

Most recently, deep learning based methods are increasingly used to address hierarchical classification [16], [23], [24], [25], [26], [40], [41]. These methods commonly fall into a multi-task learning manner, and adopt shared-specific feature representation learning to fit labels across different levels of hierarchy. Such a flexible architecture is advantageous in learning low-level features on one hand, while on the other hand, it can easily incorporate canonical inclusion relations between the parent node (super-class) and its child nodes (sub-classes) [26], [40] or exclusion relations [41] between the sibling nodes at the same hierarchy into the network design. Contrary to these works, our proposed LHT framework learns the conditional probabilities between two arbitrary nodes within adjacent hierarchies to encode the affinity relations.

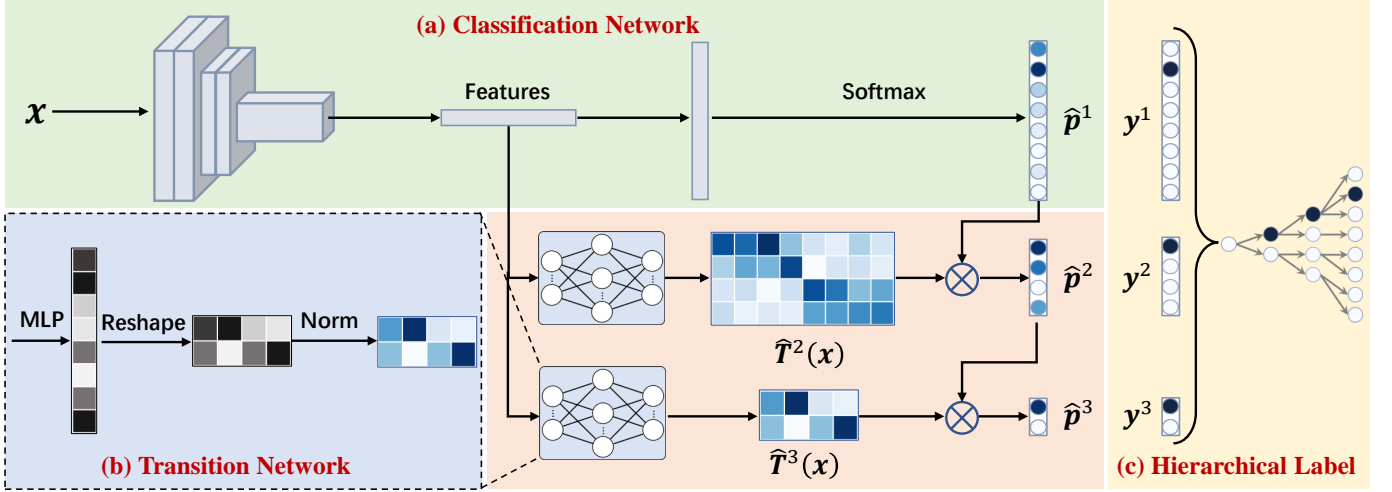


Fig. 2: Schematic illustration of the proposed LHT model. We take a three-level hierarchical classification as an example, where the number of classes within each hierarchy is 2, 4 and 8, respectively. The model consists of two key components: (i) Classification Network, which can be any existing classification network for predicting the labels of the finest-level hierarchy; (ii) Transition Network, which leverages a light-weight network (e.g., a multi-layer perceptron (MLP) with one single hidden layer) to map the feature embedding of the input sample to the label hierarchy transition matrix for each hierarchy. For each coarse-level hierarchy, its label prediction is obtained by multiplying the corresponding transition matrix by the label prediction of its adjacent fine-level hierarchy.

2.2 Hierarchical loss function

A range of literatures on hierarchical classification resorts to incorporating the class hierarchies in the loss function. In [42], the metrics associated with each node of the taxonomy tree were learned based on a probabilistic nearest-neighbour classification framework. In [43], the class hierarchies with a tree structure were used to impose prior on the parameters of the classification layer for knowledge transfer between classes, and similar strategy was proposed by Zhao et al. [20] in the traditional linear classifier. In [22], various label relations (e.g., mutual exclusion and subsumption) were encoded as conditional random field to pair-wisely capture the correlation between classes. In [44], max constraint loss was proposed to produce predictions coherent with the hierarchy constraint for addressing multi-label hierarchical classification. More recently, Bertinetto et al. [45] proposed a hierarchical loss that could be viewed as a weighted cross-entropy loss, and the weights were defined according to the depth of the label tree. In parallel to our method, Chen et al. [41] proposed a probabilistic loss to encode the label relation within each hierarchy. Our LHT model introduces a novel loss that combines the traditional cross-entropy loss with the proposed confusion loss. Different from the aforementioned methods, we aim to regularize the label hierarchy transition matrices output by our LHT model, such that class correlation from all hierarchies can be fully used to improve the classification performance.

2.3 Label embedding

Label embedding aims to encode the correlation information among classes into the traditional one-hot labels, which has been widely explored in multi-class classification [5], [6], [46], [47]. In hierarchical classification, Bertinetto et al. [17] proposed a soft-label-based method to soften the one-hot

labels according to the metric defined by the label tree. Dhall et al. [45] employed entailment cones to learn order preserving embedding, which can be embedded in both Euclidean and hyperbolic geometry enforces transitivity among class hierarchies. Although label embedding is a potential strategy to capture the correlation across class hierarchies, in this paper, we attempt to develop a unified deep classification framework for explicitly extracting correlation of hierarchical classification.

3 THE PROPOSED METHODOLOGY

In hierarchical classification tasks, a given image x is typically annotated with a sequence of K labels (y^1, y^2, \dots, y^K) , where K represents the number of label hierarchies. Each $y^k \in 1, 2, \dots, C_k$ is the label within the k -th hierarchy, with C_k denoting the number of categories within that specific hierarchy. We denote \mathbf{y}^k is the one-hot vector of y^k . Without loss of generality, we assume that the label granularity becomes coarse as k increases, i.e., $C_k > C_{k+1}$. In this paper, our goal is to propose a unified probabilistic framework to improve the accuracy of label prediction for different class hierarchies. In the following subsections, we first formulate our LHT framework that explicitly encodes the semantic correlation among hierarchies, and implement it with a classification network (Fig. 2(a)) and a transition network (Fig. 2(b)) in Sec. 3.1. We then present the architecture of the proposed transition network in Sec. 3.2. Finally, we introduce the proposed confusion loss to encourage correlation learning across hierarchies in Sec. 3.3.

3.1 Label Hierarchy Transition

The problem of interest is to directly learn the unknown classification distribution $p(y^1, \dots, y^K | x)$. We first revisit the traditional multi-task based methods in hierarchical

classification. Existing methods commonly decouple it into several multi-class classification tasks, where the label of each hierarchy is predicted by typical loss functions (e.g., cross-entropy). This is equivalent to solve the negative log-likelihood of the following equation:

$$p(y^1, \dots, y^K | \mathbf{x}) = \prod_{k=1}^K p(y^k | \mathbf{x}). \quad (1)$$

The detailed derivation can be found in Appendix A. This equation implies that all class hierarchies are statistically independent to each other, which ignores the correlation across different class hierarchies. Moreover, the cross-entropy loss with one-hot labels used in Eq. (1) inclines to overemphasize the differences among different categories but fails to depict the inter-class similarities within a specific hierarchy. Thus, the semantic correlations within the same hierarchy are also easily overlooked.

To address the aforementioned problem, we propose to explicitly encode the correlation across hierarchies into the existing multi-task learning framework. We assume that one label hierarchy y^k is statistically dependent on y^{k-1} and the sample \mathbf{x} itself, and then the distribution $p(y^k | \mathbf{x})$ can be rewritten as:

$$p(y^k | \mathbf{x}) = \sum_{y^{k-1}=1}^{C_{k-1}} p(y^k | y^{k-1}, \mathbf{x}) \cdot p(y^{k-1} | \mathbf{x}), \quad k = 2, \dots, K, \quad (2)$$

where $p(y^{k-1} | \mathbf{x})$ is the label distribution of the $(k-1)$ -th hierarchy, and $p(y^k | y^{k-1}, \mathbf{x})$ describes the transition probability from $(k-1)$ -th to k -th hierarchy, which can be viewed as the hierarchical labeling process for the k -th hierarchy according to the context of image itself and the granularity information of labeling expertise. In fact, with Eq. (2), we can readily define a fine-to-coarse learning curriculum, from which the coarser-level labels are gradually learned conditioned on the input image and its adjacent fine-grained level of labels¹. On this count, the finest-level labels should be firstly fit, which can be achieved by any existing multi-class classifier. For simplicity, we here define

$$t_{ij}^k \triangleq p(y^k = i | y^{k-1} = j, \mathbf{x}), \quad (3)$$

and then we have a $C_k \times C_{k-1}$ matrix

$$\mathbf{T}^k(\mathbf{x}) = \begin{bmatrix} t_{11}^k & t_{12}^k & \dots & t_{1C_{k-1}}^k \\ t_{21}^k & t_{22}^k & \dots & t_{2C_{k-1}}^k \\ \vdots & \vdots & \ddots & \vdots \\ t_{C_k1}^k & t_{C_k2}^k & \dots & t_{C_kC_{k-1}}^k \end{bmatrix}. \quad (4)$$

We call this matrix *Label Hierarchy Transition Matrix* (or abbreviated as *Transition Matrix*), since it defines the probability of a fine-grained label clustered to a coarse-grained label and we can get a glimpse of the *transition* status between the adjacent class hierarchies. Note that the elements of $\mathbf{T}^k(\mathbf{x})$ are positive and each column sums to 1, i.e., $\sum_{i=1}^{C_k} t_{ij}^k = 1$ for each $j \in \{1, \dots, C_{k-1}\}$.

In this paper, the core of our *Label Hierarchy Transition* model is to jointly learn the two kinds of conditional probability involved in Eq. (2) for hierarchical classification, using

1. Based on this modeling mechanism, it's natural to define a coarse-to-fine learning curriculum.

a unified deep learning framework. As shown in Fig. 2, the framework mainly consists of two components:

- *Classification Network*. As shown in Fig. 2(a), the classification network is a well-designed existing deep classification network $f_w(\cdot)$ with parameters w , e.g., ResNet-50, which is used to predict the category labels for the finest-level hierarchy of the input samples. For simplicity, we denote the predicted probability of \mathbf{x} as $\hat{\mathbf{p}}^1(\mathbf{x})$, and we thus have

$$\mathbf{p}^1(\mathbf{x}) = f_w(\mathbf{x}). \quad (5)$$

- *Transition Network*. As shown in Fig. 2(b), for hierarchy k , the transition network is designed as a lightweight network $g_{\theta_k}^k(\cdot)$ parameterized with θ_k , which generates a transition matrix $g_{\theta_k}^k(\hat{\mathbf{x}})$ to approximate the inherent transition matrices $\mathbf{T}^k(\mathbf{x})$ for the input image \mathbf{x} . Note that the proposed Transition Network takes the high-level embedding of the sample \mathbf{x} (denoted as $\hat{\mathbf{x}}$) as input, which is natural and practical since the high-level embedding is the cue to abstract \mathbf{y}^{k-1} . To simplify notation, we define $\hat{\mathbf{T}}^k(\mathbf{x}) \triangleq g_{\theta_k}^k(\hat{\mathbf{x}})$. The architecture of Transition Network will be described in detail in Sec. 3.2.

With the learned $\mathbf{p}^1(\mathbf{x})$ and $\hat{\mathbf{T}}^k(\mathbf{x})$, the predictions of k -th label hierarchy can be computed by

$$\mathbf{p}^k(\mathbf{x}) = \hat{\mathbf{T}}^k(\mathbf{x}) \mathbf{p}^{k-1}(\mathbf{x}), \quad k = 2, \dots, K. \quad (6)$$

Remark 1: From the given hierarchical labels, we can obtain a set of naive transition matrices \mathbf{S}^k , where only one element is 1 in each column, corresponding to the deterministic state transition from the finer- to the coarser-level hierarchies, i.e., $\mathbf{S}_{i,j}^k = 1$ if category j at hierarchy $k-1$ is a subclass of category i at hierarchy k , and $\mathbf{S}_{i,j}^k = 0$ otherwise. For example, in Fig. 1, the naive transition matrix form the hierarchy Species to Family is

$$\mathbf{S}^2 = \begin{bmatrix} \mathbb{1}(\text{YW} \rightarrow \text{Par}) & \mathbb{1}(\text{NW} \rightarrow \text{Par}) & \mathbb{1}(\text{RW} \rightarrow \text{Par}) & \mathbb{1}(\text{HW} \rightarrow \text{Par}) \\ \mathbb{1}(\text{YW} \rightarrow \text{Trog}) & \mathbb{1}(\text{NW} \rightarrow \text{Trog}) & \mathbb{1}(\text{RW} \rightarrow \text{Trog}) & \mathbb{1}(\text{HW} \rightarrow \text{Trog}) \end{bmatrix},$$

where $u \rightarrow v$ denote the category u at a finer-level hierarchy belongs to the category v at a coarser-level hierarchy and $\mathbb{1}$ is the indicator function that returns 1 if the statement is true and 0 otherwise. Obviously, we have $\mathbf{S}^2 = \begin{bmatrix} 1 & 1 & 0 & 0 \\ 0 & 0 & 1 & 1 \end{bmatrix}$.

Instead, in Eq. (2), we aims to model $p(y^k | y^{k-1}, \mathbf{x})$, which is a conditional label distribution considering the uncertainty from image context and hierarchy prior. For a bird image \mathbf{x} in Fig. 1, it may result in a respective transition matrix from hierarchy Species to Family:

$$\hat{\mathbf{T}}^2 = \begin{bmatrix} p(\text{Par}|\text{YW}, \mathbf{x}) & p(\text{Par}|\text{NW}, \mathbf{x}) & p(\text{Par}|\text{RW}, \mathbf{x}) & p(\text{Par}|\text{HW}, \mathbf{x}) \\ p(\text{Trog}|\text{YW}, \mathbf{x}) & p(\text{Trog}|\text{NW}, \mathbf{x}) & p(\text{Trog}|\text{RW}, \mathbf{x}) & p(\text{Trog}|\text{HW}, \mathbf{x}) \end{bmatrix}.$$

In fact, if we replace $g_{\theta_k}^k(\hat{\mathbf{x}})$ with \mathbf{S}^k in Eq. (6), the model will degenerate into only fitting the finest-level labels and it ignores the semantic correlation implied into class hierarchies, as the following theorem states.

Theorem 1. Let \mathbf{S}^k be the naive transition matrix and it satisfies that: 1) the element $\mathbf{S}_{i,j}^k = 1$ if category j at hierarchy $k-1$ is a

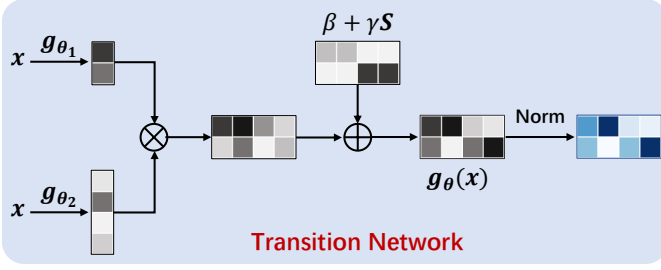


Fig. 3: Architecture of the proposed Transition Network. The network includes three small modules: two smaller MLPs g_{θ_1} and g_{θ_2} , and one bias offset term $\beta + \gamma S$. The outer product of the outputs from g_{θ_1} and g_{θ_2} , plus the bias offset term, is used to approximate the unnormalized transition matrix $g_{\theta}(\mathbf{x})$.

subclass of category i at hierarchy k and $\mathbf{S}_{i,j}^k = 0$ otherwise; 2) $\mathbf{S}^k \mathbf{y}^{k-1} = \mathbf{y}^k$. Given the hierarchical cross-entropy loss

$$\mathcal{L}_{\text{CE}} = \sum_{i=1}^N \sum_{k=1}^K \text{CE}(\hat{\mathbf{p}}^k(\mathbf{x}_i), \mathbf{y}_i^k), \quad (7)$$

where $\hat{\mathbf{p}}^k(\mathbf{x}_i) = \mathbf{S}^k \hat{\mathbf{p}}^{k-1}(\mathbf{x}_i)$, $k = 2, \dots, K$, then we have that minimizing the loss function in Eq. (7) results in a trivial solution. To be more specific, the problem (7) has exactly the same solution as the following optimization problem

$$\min_w \sum_{i=1}^N \text{CE}(\hat{\mathbf{p}}^1(\mathbf{x}_i), \mathbf{y}_i^1). \quad (8)$$

Please refer to Appendix B for the proof of the theorem.

3.2 Transition Network

A natural way to implement Transition Networks $\{g_{\theta_k}^k\}_{k=2}^K$ is to use multi-layer perceptrons (MLPs), where a separate MLP $g_{\theta_k}^k$ ($k = 2, \dots, K$) is responsible for outputting a transition matrix for one specific hierarchy. As such, the network $g_{\theta_k}^k$ outputs a $(C_k \times C_{k-1})$ -dim vector. The resulting vector is reshaped to a $C_k \times C_{k-1}$ matrix, and imposed a column-wise normalization (via *softmax* activation function) for satisfying $\sum_{i=1}^{C_k} \hat{\mathbf{T}}_{ij}^k = 1$.

However, the aforementioned strategy that uses MLPs to generate the label hierarchy transition matrices requires a large number of parameters. To prevent an explosion of parameters, we propose a simple design for $g_{\theta_k}^k$ where the MLP module is replaced with three smaller modules. In the following text, we omit subscript k for simplifying the notation. As shown in Fig. 3, two smaller MLP modules g_{θ_1} and g_{θ_2} take the high-level embedding of input sample \mathbf{x} (denoted as $\hat{\mathbf{x}}$) as input and output two small matrices $g_{\theta_1}(\hat{\mathbf{x}}) \in \mathbb{R}^{C_k \times s}$ and $g_{\theta_2}(\hat{\mathbf{x}}) \in \mathbb{R}^{s \times C_{k-1}}$, where s is a hyper-parameter. Then, the outer product of the two small matrices is used to approximate the matrix output by g_{θ} , which can be formulated as

$$g_{\theta}(\hat{\mathbf{x}}) = g_{\theta_1}(\hat{\mathbf{x}}) \otimes g_{\theta_2}(\hat{\mathbf{x}}) + \beta, \quad (9)$$

where β is a trainable scalar value that can be viewed as a bias term, and \otimes denotes outer product operation of two matrices.

Except for the context of the input image itself, the transition probability in Eq. (3) is also dependent on the granularity information of label hierarchies. Thus, we further introduce a bias offset module that simply add an offset term to the transition matrix g_{θ}^k as follows:

$$g_{\theta}(\hat{\mathbf{x}}) = (g_{\theta_1}(\hat{\mathbf{x}}) \otimes g_{\theta_2}(\hat{\mathbf{x}}) + \beta) + \gamma \mathbf{S}^k, \quad (10)$$

where γ is a trainable scalar value that scales the whole elements of the naive transition matrix \mathbf{S}^k . Finally, we perform a column-wise normalization through *softmax* function to let each column of $g_{\theta}(\hat{\mathbf{x}})$ sum to 1. Thus, the final transition matrix $\hat{\mathbf{T}}^k(\mathbf{x}_i)$ can be formulated as

$$\hat{\mathbf{T}}^k(\mathbf{x}_i) = \text{Softmax}(g_{\theta}(\hat{\mathbf{x}})), \quad (11)$$

where $\text{Softmax}(A)$ denotes column-wisely normalize the input matrix A through *softmax* function, namely, for any element A_{ij} of A , it is normalized to be $e^{A_{ij}} / \sum_i e^{A_{ij}}$.

Remark 2: From Eq. (10), we know that $\hat{\mathbf{T}}^k(\mathbf{x}_i)$

well covers the label transition information between classes across two adjacent hierarchical levels. Therefore, the transition matrix obtained from Eq. (11) is conditioned on both the context of the sample itself and the hierarchical label information. This complies with the key insight into Eq. (3).

3.3 Confusion Loss

We herein describe the optimization of the parameters involved in our approach. From Eq. (6), we get the predictions of the labels at each hierarchy, such that the parameters involved in classification network and transition network, i.e., w and θ , can be jointly optimized by the cross-entropy loss imposed on each hierarchy. Given a batch of training data $\{x_i, (y_i^1, y_i^2, \dots, y_i^K)\}_{i=1}^N$, where N is batch-size, the resulting loss function can be formulated as

$$\begin{aligned} \mathcal{L}_{\text{CE}} &= \sum_{i=1}^N \sum_{k=1}^K \text{CE}(\mathbf{p}_i^k, \mathbf{y}_i^k) \\ &= \sum_{i=1}^N \left(\text{CE}(\mathbf{p}^1(\mathbf{x}_i), \mathbf{y}_i^1) + \sum_{k=2}^K \text{CE}(\hat{\mathbf{T}}^k(\mathbf{x}_i) \mathbf{p}_i^{k-1}, \mathbf{y}_i^k) \right). \end{aligned} \quad (12)$$

As previously discussed, the proposed transition matrices play the roles to recursively predict the label distribution in a fine-to-coarse order, which to some extent imposes the correlation between class hierarchies. However, the network training by minimizing Eq. (12) remains the following challenges: (i) The manually annotated labels within each hierarchy are one-hot, and such a cross-entropy loss encourages the network to move all categories toward orthogonality at each hierarchy, counteracting the inter-class similarity introduced by class hierarchies; (ii) From the perspective of numerical optimization, there are infinite combinations of $\hat{\mathbf{T}}^2(\mathbf{x})$ and Classification Network $\mathbf{p}_w^1(\mathbf{x})$, such that \mathbf{p}^2 computed by Eq. (6) can perfectly match the given label distribution \mathbf{y}^2 for any given image \mathbf{x} .

To address the aforementioned challenges, we further introduce an additional regularization loss on transition matrices $\{\hat{\mathbf{T}}^k(\mathbf{x})\}_{k=2}^K$, which we call the confusion loss $\mathcal{L}_{\text{Conf}}$. We herein revisit the label hierarchy transition matrices

Algorithm 1 Mini-batch training algorithm of LHT

Input: Training data \mathcal{D} , hierarchy level K , batch size N , training iteration T , learning rate α .

Output: Model parameters $\{w\}$ of Classification Network and $\{\theta\}$ of Transition Network.

```

1: Initialize the parameters  $w^1$  and  $\theta^1$ .
2: for  $t = 1$  to  $T$  do
3:    $\hat{\mathcal{D}} = \{\mathbf{x}_i, y_i\}_{i=1}^N \leftarrow \text{SampleMiniBatch}(\mathcal{D}, N)$ , where
      $y_i = \{y_i^1, \dots, y_i^K\}$ .
4:   for  $k = 1$  to  $K$  do
5:     if  $k=1$  then
6:       Compute  $\hat{\mathbf{p}}^1(\mathbf{x}_i)$  by Classification Network according to Eq. (5).
7:     else
8:       Compute  $\hat{\mathbf{T}}^k(\mathbf{x}_i)$  by Transition Network according to Eq. (11).
9:       Compute  $\hat{\mathbf{p}}^k(\mathbf{x}_i)$  by Eq. (6).
10:    end if
11:  end for
12:  Compute the classification loss  $\mathcal{L}_{ce}$  by Eq. (12).
13:  Compute the confusion loss  $\mathcal{L}_{conf}$  by Eq. (13).
14:  Compute the overall training loss  $\mathcal{L}$  by Eq. (14).
15:  Update  $\{w^{t+1}, \theta^{t+1}\} = \{w^t, \theta^t\} - \alpha \nabla_{w, \theta} \mathcal{L}$ .
16: end for

```

Return: optimal parameters w^* and θ^*

involved in our LHT model. The column vector (e.g., the j -th one) of transition matrix $\hat{\mathbf{T}}^k(\mathbf{x})$ represents the label distribution of the k -th hierarchy when the sample is labeled as class j at $(k-1)$ -th hierarchy. Each element of this vector denotes the likelihood of similarity, or confusion, between two classes across two adjacent hierarchies. The proposed confusion loss aims to encourage such class confusion to counter the over-confident prediction brought about by the cross-entropy loss. Mathematically, the confusion loss is defined as the negative entropy of the column space spanned by the transition matrices, i.e.,

$$\mathcal{L}_{\text{Conf}} = \sum_{i=1}^N \sum_{k=2}^K \sum_{j=1}^{C_{k-1}} \frac{1}{C_{k-1}} \left\langle \hat{\mathbf{T}}_{\cdot j}^k(\mathbf{x}_i), \log(\hat{\mathbf{T}}_{\cdot j}^k(\mathbf{x}_i)) \right\rangle, \quad (13)$$

where $\hat{\mathbf{T}}_{\cdot j}^k(\mathbf{x}_i)$ denotes the j -th column of $\hat{\mathbf{T}}^k(\mathbf{x}_i)$, $\log(\cdot)$ is element-wise logarithm operation for vectors, and $\langle \cdot, \cdot \rangle$ is the inner product operation of vectors. Through minimization of Eq. (13), the conditional distribution represented by each column of $\hat{\mathbf{T}}^k(\mathbf{x}_i)$ is encouraged to have a higher entropy (i.e., this distribution inclines to approach uniform distribution). In other words, this introduces *confusion* in clustering a fine-grained label to a coarse-grained one during training, and eventually softens the prediction scores obtained by Eq. (6). Thus, the confusion loss can be used to alleviate the over-confident prediction brought about by the cross-entropy loss.

Combined Eq. (12) and Eq. (13), the overall training loss can be formulated as

$$\mathcal{L} = \mathcal{L}_{\text{CE}} + \lambda \mathcal{L}_{\text{Conf}}, \quad (14)$$

where λ is hyper-parameter for trade-off between the cross-entropy term \mathcal{L}_{CE} and the confusion regulation term $\mathcal{L}_{\text{Conf}}$.

All the parameters involved in our LHT can be trained in an end-to-end manner. The training algorithm is summarized in Algorithm 1.

4 EXPERIMENTAL RESULTS

In this section, we first demonstrate the effectiveness of the proposed LHT in **supervised/semi-supervised hierarchical classification** tasks following [41]. Specifically, the labels of training samples are given at all levels of the class hierarchy under the supervised setting. However, under the semi-supervised setting, the labels are observed at different levels of the class hierarchy, indicating that part of samples are only observed at internal levels of the whole hierarchies². Next, we demonstrate the applicability of the proposed LHT on **large-scale low-shot learning** where transferable visual features are learned from a class hierarchy to encode the semantic relations between source and target classes. We also provide thorough ablation studies to gain insight into our method by showing the efficacy of each key component.

4.1 Supervised/Semi-supervised Hierarchical Learning

4.1.1 Datasets

In our experiments, we evaluate our method on three public benchmark datasets: CUB-200-2011 [48], Aircraft [49] and Stanford Cars [50], where the label hierarchies are publicly available or constructed by Chang et al. [26] according to their lexical relationships in Wikipedia.

CUB-200-2011³ is a dataset of bird images mainly introduced for the problem of fine-grained visual categorisation methods. It contains 11,877 images belonging to 200 bird species. For hierarchical classification evaluation, the labels are re-organized into three-level hierarchy with 13 orders, 38 families and 200 species by tracing their biological taxonomy [26]. For example, the original label “*Brewer Blackbird*” is spanned into (“*Passeriformes*”, “*Icteridae*”, “*Brewer Blackbird*”) in the order of (Order, Family, Species).

Aircraft⁴ consists of 10,000 images across 100 airplane classes, with a data ratio of approximately 2:1 between the training and test sets. The dataset includes a three-level label hierarchy with 30 makers (e.g., “*Boeing*”), 70 families (e.g., “*Boeing 767*”) and 100 models (e.g., “*767-200*”). As a result, this dataset can be readily used in our experiments without any modification.

Stanford Cars⁵ contains 8,144 training and 8,041 test images across 196 car classes. It is re-organized into two-level label hierarchy, i.e., 9 car types and 196 car classes as introduced in [26]. For example, the class label “*BMW X6 SUV 2012*” are spanned into (“*SUV*”, “*BMW X6 SUV 2012*”). We use the standard public train/test splits, and not any bounding box/part annotations are involved in all our experiments.

2. In this paper, we stem the term of “semi-supervised learning” from [41], in the sense of “partially supervised with incomplete hierarchical labels for a part of training samples”, in contrast to the classical term that assumes most training samples are given without any annotation.

3. <http://www.vision.caltech.edu/visipedia/CUB-200-2011.html>

4. <https://www.robots.ox.ac.uk/vgg/data/fgvc-aircraft>

5. <https://www.kaggle.com/datasets/jessicali9530/stanford-cars-dataset>

TABLE 1: Comparison results of all competing methods over *ACC* and *mACC* on CUB-200-2011 dataset. *R* denotes that a fraction of *R*% of the training samples is randomly selected for label masking at the finest-level (Species) hierarchy. The best results are highlighted in **bold**. * indicates the results reported in the original paper.

<i>R</i>	Hierarchy	HD-CNN [23]		HMCN [51]		C-HMCNN [44]		FGoN [26]		HRN [41]		HRN [41]*		Ours	
		ACC	mACC	ACC	mACC	ACC	mACC	ACC	mACC	ACC	mACC	ACC	mACC	ACC	mACC
0%	Order	98.5		98.2		98.6		98.8		98.8		98.7		99.0	
	Family	95.5	93.3	94.7	93.0	95.7	93.6	95.5	93.6	95.5	93.7	95.5	93.6	96.2	94.1
	Species	85.9		86.0		86.5		86.6		86.7		86.6		87.0	
30%	Order	98.5		98.0		98.5		98.7		98.5		98.3		98.9	
	Family	95.3	92.5	94.0	91.9	95.2	92.8	95.2	93.0	95.0	92.4	94.8	92.3	96.2	93.7
	Species	83.8		83.6		84.6		85.1		83.6		83.9		86.0	
50%	Order	98.4		97.9		98.5		98.7		98.0		97.9		98.9	
	Family	94.7	91.7	93.5	90.2	94.8	91.9	95.3	92.3	94.7	91.3	94.3	90.9	96.1	93.3
	Species	81.9		79.2		82.3		82.8		81.1		80.5		84.8	
70%	Order	98.4		97.7		96.9		98.7		97.2		98.4		98.9	
	Family	94.7	90.1	92.7	87.1	91.3	87.8	94.9	90.7	93.3	88.3	93.9	88.8	96.0	92.4
	Species	77.2		70.9		75.2		78.6		74.4		74.0		82.4	
90%	Order	98.5		97.8		91.2		98.7		97.7		98.0		98.8	
	Family	94.6	83.8	90.6	79.3	77.1	72.6	94.3	85.6	93.6	83.4	93.3	81.4	95.3	87.6
	Species	58.3		49.4		49.6		63.8		58.8		53.0		68.8	

TABLE 2: Comparison results of all competing methods over *ACC* and *mACC* on Aircraft dataset. *R* denotes that a fraction of *R*% of the training samples is randomly selected for label masking at the finest-level (Model) hierarchy. The best results are highlighted in **bold**. * indicates the results reported in the original paper.

<i>R</i>	Hierarchy	HD-CNN [23]		HMCN [51]		C-HMCNN [44]		FGoN [26]		HRN [41]		HRN [41]*		Ours	
		ACC	mACC	ACC	mACC	ACC	mACC	ACC	mACC	ACC	mACC	ACC	mACC	ACC	mACC
0%	Maker	96.9		97.2		97.1		97.1		97.3		97.5		97.4	
	Family	94.9	94.3	95.6	95.1	95.4	94.6	95.5	94.7	95.7	95.2	95.8	95.3	95.9	95.3
	Model	91.1		92.6		91.4		91.4		92.7		92.6		92.6	
30%	Maker	96.9		97.2		96.3		96.9		97.3		97.3		97.2	
	Family	94.6	93.7	95.6	94.8	94.0	93.1	95.4	94.1	95.3	94.5	95.5	94.8	95.8	95.0
	Model	89.7		91.6		89.0		90.0		91.0		91.6		91.9	
50%	Maker	96.8		96.9		95.9		96.9		96.8		97.3		97.3	
	Family	94.8	93.4	95.1	93.8	93.2	92.1	95.3	93.5	95.1	94.0	95.7	94.2	95.8	94.8
	Model	88.7		89.3		87.1		88.2		90.1		89.7		91.4	
70%	Maker	96.7		96.9		93.4		96.9		96.2		96.8		97.3	
	Family	94.5	92.3	94.4	92.1	89.7	88.0	95.2	92.0	93.8	91.9	94.2	91.8	95.3	93.6
	Model	85.8		84.9		80.8		83.8		85.7		84.5		88.1	
90%	Maker	96.6		96.9		73.7		96.4		96.3		95.4		97.1	
	Family	93.8	89.0	94.7	89.1	63.0	61.6	94.6	87.6	92.5	87.3	91.7	86.1	95.0	90.5
	Model	76.7		75.8		48.1		71.9		73.2		71.1		79.3	

4.1.2 Experimental settings

We herein describe the evaluation metrics and experimental training details.

Evaluation Metrics: We adopt the same evaluation metrics as Chang et al. [26] to evaluate our method. Specifically, *ACC* (i.e., accuracy, the percentage of images whose labels are correctly classified) is reported at each class hierarchy, and then *mACC* (the mean of *ACC* across all class hierarchies) is calculated to measure the classification performance at a hierarchical level. Note that, unless otherwise specified, the *ACC* results are reported as the mean over three runs of each experiment.

Dataset Reconstruct: For the supervised hierarchical classification setting, we train the model using the complete set of labels at all hierarchical levels for each training sample. For the semi-supervised hierarchical classification

setting, in order to simulate a lack of domain knowledge, we randomly select 30%, 50%, 70%, and 90% samples (denoted as $R = 90\%$ for example) to mask out their labels at the finest-level hierarchy, such that their intermediate parent classes are relabeled as the leaf classes. When employing this approach in semi-supervised scenarios, in our model training process, we simply neglect the loss imposed on the finest-level hierarchy for the samples that have been relabeled to their parent classes.

Implementation Details: All our experiments are implemented with the Pytorch platform [52] running on NVIDIA Geforce RTX 3090Ti GPUs. Following [26], we employ ResNet-50 pre-trained on ImageNet [53] as our network backbone, followed by a fully-connected layer with 600 hidden units. For fair comparison, the features of fully-connected layer are uniformly split into K parts ($K = 2$

TABLE 3: Comparison results of all competing methods over ACC and mACC on Stanford Cars dataset. R denotes that a fraction of $R\%$ of the training samples is randomly selected for label masking at the finest-level (Maker) hierarchy. The best results are highlighted in **bold**. * indicates the results reported in the original paper.

R	Hierarchy	HD-CNN [23]		HMCN [51]		C-HMCNN [44]		FGoN [26]		HRN [41]		HRN [41]*		Ours	
		ACC	mACC	ACC	mACC	ACC	mACC	ACC	mACC	ACC	mACC	ACC	mACC	ACC	mACC
0%	Type	96.8	94.9	97.0	95.2	97.7	95.4	96.7	95.1	97.2	95.4	97.4	95.7	97.0	95.6
	Maker	93.0		93.4		93.1		93.4		93.6		94.0	94.1		
30%	Type	96.5	94.2	96.6	94.0	96.9	93.9	96.5	94.2	96.5	94.0	96.1	93.4	97.0	95.2
	Maker	91.8		91.4		90.9		91.8		91.4		90.6	93.4		
50%	Type	96.3	93.0	96.6	92.1	95.5	92.0	96.2	93.1	96.0	92.2	95.9	92.3	96.9	94.8
	Maker	89.7		87.6		88.4		90.0		88.3		88.7		92.7	
70%	Type	96.1	90.5	96.2	86.8	93.4	86.7	95.8	89.9	96.0	87.9	96.1	89.9	96.9	93.4
	Maker	84.8		77.3		80.0		84.0		79.7		83.7		89.9	
90%	Type	95.3	76.6	95.2	69.8	82.4	65.5	95.0	77.4	94.1	71.0	94.3	71.8	96.0	83.7
	Maker	57.8		44.4		48.5		59.7		47.9		49.3		71.4	

for Stanford Cars and $K = 3$ for other datasets), with each used for predicting the labels at each hierarchy. During training, the models are trained with Momentum SGD with a momentum of 0.9, a weight decay of 5×10^{-4} , a batch-size of 8, and an initial learning rate of 0.0002 for backbone layers and 0.002 for other layers. The training epoch is set to be 200 and the learning rate is adjusted by the cosine annealing schedule. We initially set $\lambda = 0.1$ for Cub-200-2011 and $\lambda = 2.0$ for the other two datasets, except for $\lambda = 0.01$ for all the three datasets under a relabeled ratio of $R = 90\%$. The same augmentation strategies as described in [41] are adopted, i.e., each image is resized to 448×448 , and then the resulting image is randomly cropped (random cropping for training and center cropping for testing) and randomly horizontally flipped.

4.1.3 Comparison Results

We compare the proposed method with state-of-the-art methods on this task, including: (i) **HD-CNN** [23], which aims to learn a hierarchical deep convolutional neural network where a single network backbone was shared by multiple fully-connected layers with each one responsible for the label prediction within one hierarchy; (ii) **HMCN** [51], which designs a specific network architecture with multiple local outputs for label prediction per hierarchical level and one global output layer for capturing semantic correlation in the hierarchy as a whole; (iii) **C-HMCNN** [44], which exploits the hierarchy information by imposing the parent-child constraint on the output of the coarser-grained hierarchies, so as to ensure that no hierarchy violation happens (i.e., when the network predicts a sample belonging to a class, this sample also belongs to its parent classes); (iv) **FGoN** [26], one of the current state-of-the-arts which equips with level-specific classification head to disentangle and reinforce the features of different class hierarchies, that is, only forces finer-grained features (with stopped gradient) to participate in coarser-grained label predictions; (v) **HRN** [41], which incorporates hierarchical feature interaction into model design and proposes a hierarchical residual network, where hierarchy-specific features from parent level are added to features of children levels through residual connections. For fair comparison, we conduct all the experiments under a unified codebase that includes: the

public source codes of C-HMCNN [44]⁶, FGoN [26]⁷ and HRN [41]⁸, and the reproduced codes of HD-CNN [23] and HMCN [51] since no source code is available for the original papers. When adapting these methods to semi-supervised settings, we neglect the loss over the leaf class if a sample has been relabeled to its parent class.

In Tab. 1, 2 and 3, we report ACC of each hierarchical level and mACC results on test sets of CUB-200-2011, Aircraft, and Stanford Cars, respectively, obtained by all competing methods. For **supervised hierarchical classification** setups (i.e., $R = 0\%$), we can observe that our LHT model consistently achieves superior or comparable performance in terms of ACC at each hierarchy, and it consistently outperforms all compared methods over mACC on all three datasets. For **semi-supervised hierarchical classification**, we select four setups (i.e., $R = 30\%, 50\%, 70\%, 90\%$) to imitate the lack of domain knowledge. Note that the dataset with $R = 30\%$ means that we randomly select 30% samples from the training set and mask out their labels at the finest-level hierarchy during training. It can be observed that: 1) Our LHT achieves the best or second best ACC and mACC performance across all the hierarchies on all the three datasets. Particularly, in cases where limited fine-grained label information ($R = 90\%$) is available, our LHT surpasses all compared methods at all hierarchies by an evident margin, resulting in absolute mACC improvements of 5.0%, 2.6%, and 13.6% compared to the second best results on all three datasets, respectively. 2) The performance of all compared methods degrade with an increasing number of relabeled samples ($R = 0\% \rightarrow 90\%$), but our LHT model consistently outperforms current state-of-the-art methods. This indicates that LHT can better utilize hierarchical label information to learn a more discriminative classifier. 3) To elucidate the origins of performance improvements, we visually represent the confusion matrices obtained from the test set of Cub-200-2011 dataset, employing a relabeled ratio of $R = 90$. It should be noted that the diagonal vector of a confusion matrix signifies per-class recall. As shown in Fig. 4, our LHT model exhibits a notably superior improve-

6. <https://github.com/EGiunchiglia/C-HMCNN>

7. <https://github.com/PRIS-CV/Fine-Grained-or-Not>

8. <https://github.com/MonsterZhZh/HRN>

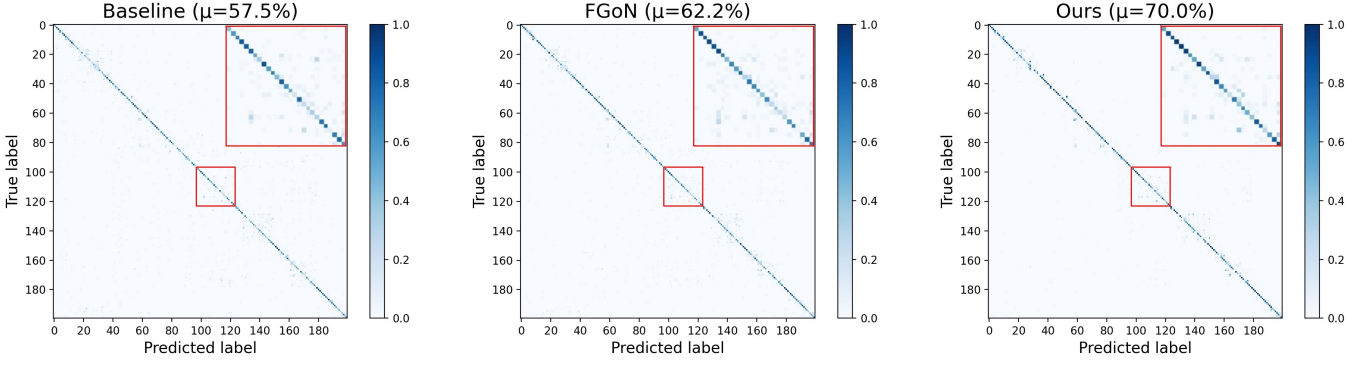


Fig. 4: Confusion matrices of Baseline, FGoN [26] and our proposed LHT method (Ours) at the finest-grained hierarchy on Cub-200-2011 with the relabeled ratio $R = 90$. Here μ above each figure represents mean-class-recall for all 200 classes.

TABLE 4: Ablation study on each key component of the proposed LHT model. The performance (ACC) is evaluated at the finest-level (Species) hierarchy through incremental integration of Hierarchical Cross-entropy Loss (HCL), Transition Network, and Confusion Loss into the backbone ResNet-50.

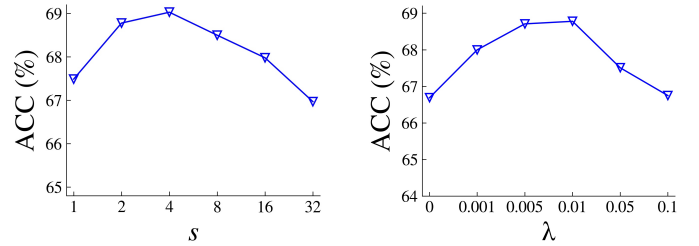
ResNet-50	HCL	Transition Network	Confusion Loss	ACC
✓				55.9
✓	✓			58.3
✓	✓	✓		66.7
✓	✓	✓	✓	68.8

ment compared to the baseline model ResNet-50 and the current state-of-the-art method FGoN [26]. Specifically, LHT achieves a mean-class-recall (defined as the arithmetic mean of the recalls across all 200 classes) of 70.0%, surpassing the baseline and FGoN by 12.5% and 7.8%, respectively. These results substantiate the superiority of our proposed method in effectively capturing hierarchical knowledge during the training process.

4.1.4 Ablation study

We perform extensive ablation study to evaluate and understand the contribution of each critical component in the proposed LHT model. Unless mentioned otherwise, the experiments in this subsection are all performed on Cub-200-2011 dataset with relabeled ratio $R = 90\%$.

Effect of Label Hierarchy. We first investigate the impact of label hierarchy to demonstrate that hierarchical label information is beneficial for performance enhancement, but it requires effective learning mechanisms to exploit its underlying semantics. To this end, we append a branch for each hierarchy level on ResNet-50 and use the hierarchical cross-entropy loss (denoted as ResNet-50 + HCL) to fit the labels at each hierarchy, and the results are listed in Tab. 4. It can be observed that the performance only exhibits a marginal improvement of about 2.4%, indicating a limited boost in comparison to the advancements achieved by our proposed LHT model. Moreover, in Sec. 4.1.5, we will further demonstrate that our proposed LHT model can effectively utilize hierarchical label information in a more



(a) Test performance (ACC) with different s values.

(b) Test performance (ACC) with different λ values.

Fig. 5: Ablation study on two hyper-parameters: (a) s in the transition network and (b) λ in the training loss (Eq. (14)).

sparse annotation scenario, in which the labels of the two finest-level hierarchies will be masked out.

Effect of Transition Network. We herein validate the superiority of the proposed transition network, which exhibits the potential to effectively encodes the intrinsic correlation embedded within class hierarchies, as delineated in Sec. 3.2. With this end, we quantify the performance of the model (ResNet-50 + HCL + Transition Net) that augments ResNet-50 with our proposed transition network, yet is trained solely with the hierarchical cross-entropy loss. The results in Tab. 4 show that our proposed transition network achieves an ACC performance of 66.7%, resulting in a substantial absolute performance gain of up to 8.4% compared with the baseline model (ResNet-50 + HCL). This substantiates the efficacy of our proposed transition network in enhancing classification performance through the integration of hierarchical correlations. Besides, the transition network introduces the hyper-parameter s to constrain the model capacity. As shown in Fig. 5(a), we can see that the performance remains relatively stable as the value of s varies. As such, we fix it as 2 across all our experiments for a better trade-off between computation efficiency and model performance.

Effect of Confusion Loss. We further conduct ablation analysis on the proposed confusion loss. As shown in Tab. 4, when the confusion loss is integrated into the model (ResNet-50 + HCL + Transition Net), the resulting LHT model (ResNet-50 + HCL + Transition Net + Confusion Loss) achieves a further 2.1% performance improvement.

TABLE 5: Analysis for more sparse annotation settings on CUB-200-2011 dataset. R^2 denotes that a fraction of $R\%$ of the training samples is randomly selected for label masking at the two finest-level (Species and Family) hierarchies.

R^2 (%)	Hierarchy	Baseline		Ours	
		ACC	mACC	ACC	mACC
30	Order	98.5		98.9	
	family	94.5	92.3	95.9	93.4
	Species	83.8		85.3	
50	Order	98.4		98.9	
	Family	93.4	91.1	95.6	92.9
	Species	81.4		84.3	
70	Order	98.4		98.8	
	Family	91.1	88.2	94.8	91.6
	Species	75.2		81.1	
90	Order	97.9		98.3	
	Family	82.4	77.1	85.6	81.4
	Species	51.0		60.4	

This verifies the effectiveness of the proposed confusion loss on encouraging the transition network to capture the semantic correlation within class hierarchies. In fact, the hyper-parameter λ in Eq. (14) plays an important role in trading off between the hierarchical cross-entropy loss and the confusion loss during training, and we thus conduct a detailed ablation analysis on λ in Fig. 5(b). It can be observed that the initial performance gradually improves as λ increase from 0 to 0.01, which suggests that a smaller λ facilitates the transfer network to output meaningful transfer matrices; however, a much larger λ excessively forces the output transfer matrices to be more smooth, which may amplify biases introduced by inaccurate predictions, especially in semi-supervised scenarios.

4.1.5 Analysis and Discussion

In order to gain a deeper understanding of the effectiveness underlying the proposed LHT model, we herein address the following questions.

How does LHT perform under more sparse annotation settings? As aforementioned, our proposed LHT model presents an effective learning mechanism to exploit hierarchical label information, especially in cases where a significant portion of labels at the finest-level hierarchy is missing. Herein, we further validate the efficacy of our method in a more challenging semi-supervised scenario, where we randomly select a fraction of samples and mask out their labels at the two finest-level hierarchies (i.e., Species and Family) on Cub-200-2011 dataset. As shown in Tab. 5, Our proposed LHT model consistently improves the baseline HD-CNN [23] across different amounts of relabeled data. For example, in an extremely sparse annotation scenario ($R^2 = 90\%$), LHT significantly improves the baseline model by around 9.4% ACC at the finest-level hierarchy and 4.3% mACC across all hierarchies. Interestingly, the performance of our LHT under $R^2 = 90\%$ is even higher than that of the baseline model under $R = 90\%$ where more annotations are given at the Family hierarchy (Refer to Tab. 1 for the result), and improves by $58.3 \rightarrow 60.4$ at the finest-level hierarchy. This demonstrates that our LHT achieves higher

TABLE 6: Comparison with FGON [26] across different datasets ($R = 100\%$) under the low-resolution input settings. * indicates the results reported in the original paper.

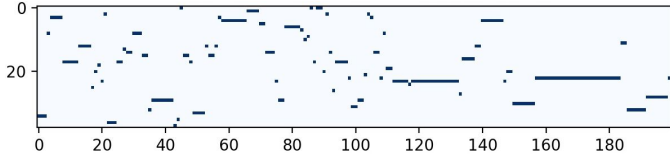
Dataset	Hierarchy	FGON*		Ours	
		ACC	mACC	ACC	mACC
Cub-200-2011	Order	96.4		97.7	
	Family	90.4	88.2	92.3	90.0
	Species	78.0		79.9	
Aircraft	Maker	93.0		95.6	
	Family	90.7	90.7	93.4	92.8
	Model	88.4		89.4	
Stanford Cars	Type	95.6		96.1	
	Maker	89.7	92.7	90.4	93.3

performance with less label information, thus confirming its superiority in effectively utilizing class hierarchies.

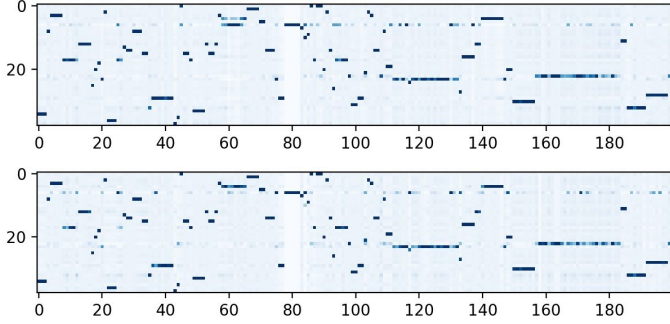
How does LHT perform when meeting low-resolution images? As investigated in [26], low-resolution images may potentially degrade the performance of a hierarchical classification system, and the proposed FGON [26] shows evident superiority to take advantage of hierarchical label information, thus mitigating the harm brought about by the image quality. To validate the effectiveness of the proposed method in low-resolution images settings, we directly compare with FGON following the same training protocols. Concretely, we reduce the image resolution to 224×224 , and keep other settings unchanged for fair comparison. As shown in Tab. 6, our proposed LHT model consistently surpasses FGON, and achieves absolute mACC gains of 1.8%, 2.1% and 0.6% on Cub-200-2011, Aircraft and Stanford Cars datasets, respectively. This verifies that our method has fine potential to infer category labels from class hierarchies, so as to alleviate the practical limitations arising from image quality.

Does the learned label hierarchy transition matrix encode semantic correlations? To answer this question, we visualize the transition matrices outputted by the Transition Network on Cub-200-2011 dataset in Fig. 6. Specifically, we show the learned transition matrix associated with the two finest-level hierarchies, denoted as $\mathbf{T}^1(\text{species} \rightarrow \text{family})$, and also visualize the corresponding naive transition matrices $\mathbf{S}^1(\text{species} \rightarrow \text{family})$ directly inferred from hierarchical labels (as mentioned in **Remark 1**) for better reference. We can see that the naive transition matrix can only encode the deterministic state transition from the finer- to the coarser-level hierarchies since only one element is 1 in each column, whereas the ones learned from our proposed LHT model are indeed conditional label distributions considering the uncertainty from image context and hierarchy prior. This is mainly because, on one hand, our learned transfer matrices most likely respond to the transition states in the naive transfer matrix; on the other hand, our LHT model outputs different transition matrices for different input samples.

Does the learned attention map encode semantic correlations? In Fig. 7, we further employ Grad-Cam [54] to visualize the attention regions of each hierarchical branch by propagating their respective gradients back to feature maps for four typical examples. These objects belong to the same order (i.e., “Charadriiformes”), two families (i.e., “Laridae”



(a) Naive transition matrix \mathbf{S}^1 (*species* \rightarrow *family*) inferred from hierarchical labels.



(b) Learned transition matrices \mathbf{T}^1 (*species* \rightarrow *family*) for two different samples.

Fig. 6: Comparison on the visualization of (a) the naive transition matrix and (b) two learned transition matrices for two different samples on Cub-200-2011 dataset.

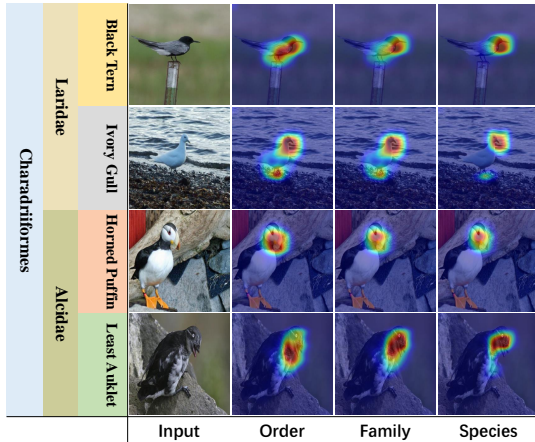


Fig. 7: Visualization of the attention maps returned by Grad-Cam [54] of the three hierarchical branches of the proposed LHT model, with each one corresponding to a specific hierarchy. The leftmost column is the original image, and the three columns on the right correspond to the attention maps of Order, Family and Species hierarchy, respectively.

and “*Alcidae*”), and four species (i.e., “*Black Tern*”, “*Ivory Gull*”, “*Least Auklet*” and “*Horned Puffin*”). It can be observed that 1) our proposed LHT model exhibits a preference for activating more global attention regions in the coarser-level hierarchy compared to the finer-level hierarchy, and the visualization results demonstrate notable difference between the attention patterns of the finer-level categories and that of the coarser-level categories; 2) our LHT model effectively directs attention towards discriminative regions when classifying examples from different species within the same family. For instance, when distinguishing between the

species “*Least Auklet*” and “*Horned Puffin*”, both belonging to the family “*Alcidae*”, the model focuses intensely on the head, particularly the eye and beak regions, which provide essential discriminative information. This further validates the capability of our LHT model in capturing semantic correlations across different hierarchies to some extent.

4.2 Low-shot Learning with Class Hierarchy

The focus of large-scale low-shot learning (LSL) problem in this work is to learn a deep feature embedding model by exploiting a class hierarchy shared by both source and target classes following [55].

4.2.1 Problem definition

Large-scale LSL problem is defined as follows. Let S_{source} denote the set of source classes and S_{target} denote the set of target classes. The two class sets satisfy the following properties: 1) S_{source} and S_{target} are disjoint, i.e., $S_{source} \cap S_{target} = \emptyset$; 2) the semantic correlation of S_{source} and S_{target} are explicitly encoded into a tree-like class hierarchy, where the leaf nodes cover all the target and source classes and the parent nodes grouped by certain leaf classes represent their semantic similarities. We are given a large-scale source set \mathcal{D}_{source} from source classes S_{source} , a few-shot support set \mathcal{D}_{target} from target classes S_{target} , and a test set \mathcal{D}_{test} from target classes S_{target} . In the LSL setting, \mathcal{D}_{source} contains sufficient labeled samples for each source class, while \mathcal{D}_{target} contains only a few (e.g., 5) labeled samples for each target class. The primary target of large-scale LSL is to predict the labels for \mathcal{D}_{test} .

4.2.2 Method formulation

Following [55], a hierarchical classification network used for large-scale LSL includes a two-stage process: 1) Training stage, in which only source class samples are used to train the hierarchical network. Since the source classes and target classes share certain common super-classes, the network facilitates the learning of transferable features for LSL on the target classes. 2) Test stage, in which visual features of the few-shot support samples and the test samples (both from target classes) are extracted through the learned hierarchical classification network. The test samples are then recognized by a simple nearest neighbor search using the visual features of the support samples as the references. Specifically, when adapting the proposed LHT method to large-scale LSL, we train the hierarchical classification network with the source data in the training stage and employ the features from global average pooling as input for the nearest-neighbor classifier in the test stage.

4.2.3 Dataset and settings

A benchmark derived from ILSVRC2012/2010 [53] is used for performance evaluation [55]. This dataset consists of three parts: a support set with 1000 source classes from ILSVRC2012, a few-shot support set with 360 target classes from ILSVRC2010 (not included in ILSVRC2012), and a test set containing target class samples excluding those in the support set. Following [55], we construct a class hierarchy with three levels according to: 1) we first cluster

TABLE 7: Comparison results for large-scale LSL on ILSVRC2012/2010 dataset. The best results are highlighted in **bold**.

Methods	<i>K</i> -shot				
	<i>K</i> = 1	<i>K</i> = 2	<i>K</i> = 3	<i>K</i> = 4	<i>K</i> = 5
NN	34.2	43.6	48.7	52.3	54.0
SGM [57]	31.6	42.5	49.0	53.5	56.8
PPA [58]	33.0	43.1	48.5	52.5	55.4
LSD [59]	33.2	44.7	50.2	53.4	57.6
KT [55]	39.0	48.9	54.9	58.7	60.5
LHT (Ours)	41.9	52.2	58.6	61.6	63.7

the word vectors⁹ of source/target class names using k-means to create a coarser-level hierarchy, and the super-class word vectors are obtained by averaging the word vectors of their child classes; 2) we then acquire upper-layer nodes by clustering the word vectors of the lower-layer nodes. These three hierarchies have 1000, 100, and 10 classes, respectively. We refer to [55] and employ Momentum SGD with a momentum of 0.9, a weight decay of 5×10^{-4} , a batch-size of 128, and an initial learning rate of 0.001 for backbone layers and 0.01 for other layers to train the model for 5 epochs. The top-5 accuracy on \mathcal{D}_{test} is adopted as the evaluation metric.

4.2.4 Comparison results

We compare our model with five large-scale LSL models: (i) NN, a baseline model employing ResNet50 pre-trained on \mathcal{D}_{source} as the nearest neighbor (NN) classifier; (ii) SGM [57], a LSL model using the squared gradient magnitude (SGM) loss [7]; (iii) PPA [58], the parameter prediction with activation (PPA) model; (iv) LSD [59], a LSL model with large-scale diffusion (LSD); (v) KT [55], the state-of-the-art LSL model via knowledge transfer (KT) with class hierarchy. The results in Tab. 7 show that our proposed LHT method achieves the best result among all the comparison methods, and the performance gain is evident compared to KT that also uses class hierarchies for LSL. This verifies the effectiveness of our proposed method in leveraging class hierarchy to facilitate large-scale LSL.

5 EXTENSION TO SKIN LESION DIAGNOSIS

In this section, we empirically shed light on the potential of the proposed LHT applied in the domain of computer-aided diagnosis. Concretely, we reformulate the lesion diagnosis problem into a hierarchical classification task, as we can readily obtain a hierarchical categorization of lesions based on pathological priors [33], [60].

5.1 Dataset and experimental settings

Dataset. The proposed model is evaluated on the publicly available ISIC2018 dataset [61] from the ISIC’2018 challenge on skin lesion diagnosis¹⁰. It is a challenging dataset due to the class-imbalanced issue. The dataset contains totally

TABLE 8: Summary of the ISIC2018 dataset. The corresponding skin lesions are organized into three levels of class hierarchies.

Category	Number	Class Hierarchy			
		Melanocytic		Non-melanocytic	
		Benign	Malignant	Benign	Malignant
NV	6705	✓			
MEL	1113		✓		
BKL	1098			✓	
BCC	514				✓
AKIEC	327				✓
VASC	143			✓	
DF	115			✓	

10015 dermoscopic images for seven skin diseases, namely Melanocytic Nevi (NV), Melanoma (MEL), Benign Keratosis (BKL), Basal Cell Carcinoma (BCC), Actinic Keratosis / Bowens disease (AKIEC), Vascular Lesion (VASC), and Dermatofibroma (DF). We organize these seven skin lesions into three hierarchies according to their origin (melanocytic or non-melanocytic), degree of malignancy (benign or malignant), and finally their diagnosis (e.g., melanoma, basal cell carcinoma, vascular lesion, etc.) following [60], [62]. In Tab. 8, we list the statistics and class hierarchies of the dataset. Since the ground truth of official validation and testing set was not released, we randomly split the entire training set to 70% for training, 10% for validation and 20% for testing. To verify the proposed method can notably improve the performance of skin lesion diagnosis and concurrently reduce the annotation cost of training samples, we conduct experiments in a semi-supervised learning regime, i.e., randomly selecting 80% of training samples and masking out their labels at the finest-level hierarchy ($R = 80\%$) or the two finest-level hierarchies ($R^2 = 80\%$).

Evaluation Metrics. To quantitatively evaluate the proposed method, we adopt five metrics, including Precision, Recall, F1-score, AUC¹¹ and Accuracy for evaluation. We report the averaged results from five independent runs with different random initialization.

Implementation details. We employ ResNet-50 pre-trained on ImageNet [53] as our network backbone, and train the models with Momentum SGD with a momentum of 0.9, a weight decay of 5×10^{-4} , a batch-size of 8, and an initial learning rate of 0.0002 for backbone layers and 0.002 for other layers. The training epoch is set as 200 and the learning rate is decayed by the cosine annealing schedule. The hyper-parameter λ in Eq. 14 is set as 0.01. In all our experiments, we resize input images to 448×448 (originally around 600×450 pixels) and simply apply random horizontal flipping and random cropping (random cropping for training and center cropping for testing) for data augmentation.

5.2 Experimental results

To understand the effectiveness of the proposed LHT applied to skin lesion diagnosis, we herein answer the following research questions under both $R = 80\%$ and $R^2 = 80\%$

⁹. The word vectors are obtained by a skip-gram text model [56] in [55] and available at <https://github.com/tiangelo/fsl-hierarchy>.

¹⁰. <https://challenge2018.isic-archive.com>

¹¹. Each metric is calculated as the average value across all classes.

TABLE 9: Per-class recall (%) on the test set of ISIC2018 dataset. R and R^2 represent the random selection of $R\%$ training samples for label masking at the finest-level and two finest-level hierarchies, respectively.

Method	Training Data		Lesion Category							Avg.
	Labeled	Patially-labeled	NV	MEL	BKL	BCC	AKIEC	VASC	DF	
ResNet-50	20%	0	94.1	42.4	60.1	68.7	68.7	77.9	58.2	67.2
LHT (Ours)	20%	$R = 80\%$	97.1	63.3	80.4	87.7	78.8	89.7	80.0	82.4
LHT (Ours)	20%	$R^2 = 80\%$	96.4	42.7	74.1	81.0	77.6	86.2	72.9	75.8

TABLE 10: Comparison results over Precision, Recall, Accuracy, F1-Score and AUC on ISIC2018 dataset. R and R^2 represent the random selection of $R\%$ training samples for label masking at the finest-level and two finest-level hierarchies, respectively. The best and second best results are highlighted in **bold** and underline, respectively.

Method	ISIC2018 ($R = 80\%$)					ISIC2018 ($R^2 = 80\%$)				
	Precision	Recall	Accuracy	F1-Score	AUC	Precision	Recall	Accuracy	F1-Score	AUC
HD-CNN [23]	79.8	<u>79.9</u>	<u>89.8</u>	<u>79.4</u>	97.3	73.4	73.0	84.9	72.3	95.1
HMCN [51]	78.5	72.2	86.6	74.3	94.5	66.6	48.4	78.0	53.7	85.9
C-HMCNN [44]	<u>80.2</u>	78.2	89.4	78.8	<u>97.5</u>	<u>73.6</u>	72.4	<u>85.4</u>	72.1	<u>95.8</u>
FGoN [26]	78.8	78.2	88.5	77.8	96.9	72.9	<u>73.7</u>	84.9	<u>72.7</u>	95.1
HRN [41]	77.7	77.6	88.6	77.1	96.4	72.8	71.5	83.9	71.8	94.3
LHT (Ours)	81.3	82.4	90.1	81.3	98.2	76.4	75.8	86.1	75.3	96.7

settings: 1) Does LHT contribute to the diagnosis of skin lesions by using class hierarchy? 2) How does LHT perform compared with prior hierarchical classification methods when used in skin lesion diagnosis?

To answer the first question, we report the per-class recall results for all the seven classes and compare it with a vanilla model (ResNet-50 without using hierarchical label information to train the model) in Tab. 9. It can be observed that: 1) Our proposed LHT method consistently improves the recall of each lesion category and improve the average recall by $67.2\% \rightarrow 82.4\%$ under $R = 80\%$ and $67.2\% \rightarrow 75.8\%$ under $R^2 = 80\%$, respectively. This demonstrates that our approach effectively leverages semantic correlations within the label hierarchy to enhance the performance of skin lesion diagnosis. 2) In the setting of $R^2 = 80\%$, it only requires coarse-level annotations (just identifying whether the lesion is melanocytic or non-melanocytic) for 80% of training data, and our LHT model results in an absolute performance gain of up to 8.6%. This highlights the significant potential of our method to reduce the annotation cost for computer-aided diagnosis systems.

In Tab. 10, we further compare the proposed LHT with state-of-the-art methods for skin lesion diagnosis on ISIC2018 dataset. The comparison methods include HD-CNN [23], HMCN [51], C-HMCNN [44], FGoN [26], and HRN [41], which are described in detail in Sec. 4.1.3. The results show that our LHT model consistently outperforms all comparison methods over all five evaluation metrics. For example, we surpass the second best result by $79.9\% \rightarrow 82.4\%$ under $R = 80\%$ and $73.7\% \rightarrow 75.8\%$ under $R^2 = 80\%$ on recall, highlighting that the proposed LHT method indeed helps to exploit the coarsely annotated hierarchical labels for skin lesion diagnosis. This reveals that our method can effectively leverage the training data annotated at different hierarchical levels to train a computer-aided diagnosis system. As such, the annotators may only need to provide partial labels with the highest confidence based on their own expertise, rather than annotating every sample into the

finest-level label, which largely alleviates the conformation bias arising from noisy labels during training.

6 CONCLUSION AND DISCUSSION

In this work we have proposed a probabilistic approach to address the hierarchical classification problem. Our key insight is to directly encode the correlation between two adjacent class hierarchies as conditional probabilities, such that the category labels across different hierarchies can be recursively predicted in a fine-to-coarse order. Beyond that, we have designed a confusion loss to further encourage the deep classifiers to learn the hierarchical correlation. We demonstrate the superiority of our method in hierarchical classification on a series of benchmark datasets and further shed light on the potential of the proposed method in computer-aided diagnosis empirically. In the future, we will further investigate the applicability of our method in a broader range of machine learning problems. For example, we will explore how to extend the method to multi-label classification tasks and evaluate its performance on more large-scale computer-aided diagnosis tasks.

APPENDIX A

DERIVATION OF EQUATION (1)

In this section, we provide a detailed derivation of the equivalence between hierarchical cross-entropy loss (i.e., the sum of cross-entropy loss for each hierarchy) and negative log-likelihood of Eq. (1). For convenience, we rewrite it here:

$$p(y^1, \dots, y^K | \mathbf{x}) = \prod_{k=1}^K p(y^k | \mathbf{x}). \quad (1)$$

Derivation. We first denote \mathbf{y}^k as the one-hot vector of y^k , \mathbf{p}^k as the corresponding prediction of y^k , and $\mathbf{v}[i]$ as the i -th element of vector \mathbf{v} . We then have

$$\begin{aligned}
& -\log p(y^1, \dots, y^K | \mathbf{x}) \\
&= -\log \prod_{k=1}^K p(y^k | \mathbf{x}) \\
&= -\sum_{k=1}^K \log p(y^k | \mathbf{x}) \\
&= -\sum_{k=1}^K \log \prod_{i=1}^{C_k} (\mathbf{p}^k[i])^{y^k[i]} \\
&= -\sum_{k=1}^K \sum_{i=1}^{C_k} y^k[i] \log \mathbf{p}^k[i] \\
&= \sum_{k=1}^K \text{CE}(\mathbf{y}^k, \mathbf{p}^k).
\end{aligned} \tag{15}$$

Note that to the right of the third equal sign, it implies that the prediction at each hierarchy follows a categorical distribution.

APPENDIX B

PROOF OF THEOREM 1

In this section, we provide the proof of Theorem 1 in detail. For convenience, we rewrite the theorem as follows:

Theorem 1. Let \mathbf{S}^k be the naive transition matrix and it satisfies that: 1) the element $\mathbf{S}_{i,j}^k = 1$ if category j at hierarchy $k-1$ is a subclass of category i at hierarchy k and $\mathbf{S}_{i,j}^k = 0$ otherwise, and 2) $\mathbf{S}^k \mathbf{y}^{k-1} = \mathbf{y}^k$. Given the hierarchical cross-entropy loss

$$\mathcal{L}_{\text{CE}} = \sum_{i=1}^N \sum_{k=1}^K \text{CE}(\hat{\mathbf{p}}_i^k, \mathbf{y}_i^k), \tag{7}$$

where $\hat{\mathbf{p}}^k = \mathbf{S}^k \hat{\mathbf{p}}^{k-1}$, $k = 2, \dots, K$, then we have that minimizing the loss function in Eq. (7) results in a trivial solution. To be more specific, the problem (7) has exactly the same solution as the following optimization problem

$$\min_w \sum_{i=1}^N \text{CE}(\hat{\mathbf{p}}^1(\mathbf{x}_i), \mathbf{y}_i^1). \tag{8}$$

Proof. We first prove that the optimal solution of Eq. (8) minimizes Eq. (7). The cross-entropy loss in Eq. (8) is bounded below by zero. If there exists w^* such that the zero loss value in Eq. (8) can be achieved¹² then we have $\hat{\mathbf{p}}^1(\mathbf{x}_i) = \mathbf{y}_i^1$ and correspondingly $\hat{\mathbf{p}}^1 = \mathbf{y}^1$. Meanwhile, we have $\mathbf{S}^2 \mathbf{y}^1 = \mathbf{y}^2$ by the property of \mathbf{S}^1 , which implies $\mathbf{S}^2 \hat{\mathbf{p}}^1 = \mathbf{y}^2$. By analogy, we have $\mathbf{S}^k \hat{\mathbf{p}}^{k-1} = \mathbf{y}^k$ for $k \in \{2, \dots, K\}$, and the loss value in Eq. (7) becomes zero, and then the optimal solution w^* of problem Eq. (8) is also the optimal solution of Eq. (7).

Now we prove that the optimal solution of Eq. (7) minimizes Eq. (8). This can be easily verified. On one hand, in Eq. (7) we have $\text{CE}(\mathbf{S}^k \hat{\mathbf{p}}^{k-1}, \mathbf{y}_i^k) \geq 0$ for $k \in \{2, \dots, K\}$ and the zero loss can only be obtained by minimizing the cross-entropy loss of each hierarchy to zero, which then proves the results. On the other hand, given the cross-entropy loss of the k -th hierarchy as $\text{CE}(\mathbf{S}^k \hat{\mathbf{p}}^{k-1}, \mathbf{y}_i^k)$, if the

loss value is minimized to zero by \hat{w} , we have $\mathbf{S}^k \hat{\mathbf{p}}^{k-1} = \mathbf{y}_i^k$. If \hat{w} does not result in zero loss of Eq. (8), one can find a direction to move w towards w^* such that the equation $\mathbf{S}^k \hat{\mathbf{p}}^{k-1} = \mathbf{y}_i^k$ holds and the problem Eq. (8) is minimized as well. \square

REFERENCES

- [1] Y. LeCun, Y. Bengio, and G. Hinton, "Deep learning," *Nature*, vol. 521, no. 7553, pp. 436–444, 2015.
- [2] A. Krizhevsky, I. Sutskever, and G. E. Hinton, "ImageNet classification with deep convolutional neural networks," *NeurIPS*, vol. 25, pp. 1097–1105, 2012.
- [3] K. Simonyan and A. Zisserman, "Very deep convolutional networks for large-scale image recognition," *ICLR*, 2015.
- [4] K. He, X. Zhang, S. Ren, and J. Sun, "Deep residual learning for image recognition," in *CVPR*, 2016, pp. 770–778.
- [5] C. Szegedy, V. Vanhoucke, S. Ioffe, J. Shlens, and Z. Wojna, "Rethinking the inception architecture for computer vision," in *CVPR*, 2016, pp. 2818–2826.
- [6] R. Müller, S. Kornblith, and G. E. Hinton, "When does label smoothing help?" *NeurIPS*, vol. 32, pp. 4694–4703, 2019.
- [7] G. A. Miller, R. Beckwith, C. Fellbaum, D. Gross, and K. J. Miller, "Introduction to wordnet: An on-line lexical database," *International journal of lexicography*, vol. 3, no. 4, pp. 235–244, 1990.
- [8] H. Bannour and C. Hudelot, "Hierarchical image annotation using semantic hierarchies," in *Proceedings of the 21st ACM International Conference on Information and Knowledge Management*, 2012, pp. 2431–2434.
- [9] L.-J. Li, C. Wang, Y. Lim, D. M. Blei, and L. Fei-Fei, "Building and using a semantivisual image hierarchy," in *CVPR*, 2010, pp. 3336–3343.
- [10] M. Marszałek and C. Schmid, "Constructing category hierarchies for visual recognition," in *ECCV*, 2008, pp. 479–491.
- [11] J. Sivic, B. C. Russell, A. Zisserman, W. T. Freeman, and A. A. Efros, "Unsupervised discovery of visual object class hierarchies," in *CVPR*, 2008, pp. 1–8.
- [12] Y. Wang, Q. Hu, P. Zhu, L. Li, B. Lu, J. M. Garibaldi, and X. Li, "Deep fuzzy tree for large-scale hierarchical visual classification," *IEEE Transactions on Fuzzy Systems*, vol. 28, no. 7, pp. 1395–1406, 2019.
- [13] J. Deng, A. C. Berg, K. Li, and L. Fei-Fei, "What does classifying more than 10,000 image categories tell us?" in *ECCV*, 2010, pp. 71–84.
- [14] R. Babbar, I. Partalas, E. Gaussier, and M. R. Amini, "On flat versus hierarchical classification in large-scale taxonomies," *Advances in neural information processing systems*, vol. 26, 2013.
- [15] R. Babbar, I. Partalas, E. Gaussier, M.-R. Amini, and C. Amblard, "Learning taxonomy adaptation in large-scale classification," *The Journal of Machine Learning Research*, vol. 17, no. 1, pp. 3350–3386, 2016.
- [16] H. Wu, M. Merler, R. Uceda-Sosa, and J. R. Smith, "Learning to make better mistakes: Semantics-aware visual food recognition," in *ACM MM*, 2016, pp. 172–176.
- [17] L. Bertinetto, R. Mueller, K. Tertikas, S. Samangooei, and N. A. Lord, "Making better mistakes: Leveraging class hierarchies with deep networks," in *CVPR*, 2020, pp. 12 506–12 515.
- [18] A. Zweig and D. Weinshall, "Exploiting object hierarchy: Combining models from different category levels," in *ICCV*, 2007, pp. 1–8.
- [19] R. Fergus, H. Bernal, Y. Weiss, and A. Torralba, "Semantic label sharing for learning with many categories," in *ECCV*, 2010, pp. 762–775.
- [20] B. Zhao, L. Fei-Fei, and E. P. Xing, "Large-scale category structure aware image categorization," in *NeurIPS*, 2011, pp. 1251–1259.
- [21] B. Liu, F. Sadeghi, M. Tappen, O. Shamir, and C. Liu, "Probabilistic label trees for efficient large scale image classification," in *CVPR*, 2013, pp. 843–850.
- [22] J. Deng, N. Ding, Y. Jia, A. Frome, K. Murphy, S. Bengio, Y. Li, H. Neven, and H. Adam, "Large-scale object classification using label relation graphs," in *ECCV*, 2014, pp. 48–64.
- [23] Z. Yan, H. Zhang, R. Piramuthu, V. Jagadeesh, D. DeCoste, W. Di, and Y. Yu, "Hd-cnn: hierarchical deep convolutional neural networks for large scale visual recognition," in *ICCV*, 2015, pp. 2740–2748.

12. Note that for $\text{CE}(\mathbf{p}(x), \mathbf{y})$, as $\mathbf{p}(x)$ is obtained by applying the softmax function to the logits \mathbf{z} , defined as $\mathbf{p}(x) = \frac{e^{\mathbf{z}_y}}{\sum_{i=1}^{K} e^{\mathbf{z}_i}}$, by 'zero loss' we mean that $\mathbf{z}_y \rightarrow \infty$.

- [24] A. Bilal, A. Jourabloo, M. Ye, X. Liu, and L. Ren, "Do convolutional neural networks learn class hierarchy?" *IEEE TVCG*, vol. 24, no. 1, pp. 152–162, 2017.
- [25] T. Chen, W. Wu, Y. Gao, L. Dong, X. Luo, and L. Lin, "Fine-grained representation learning and recognition by exploiting hierarchical semantic embedding," in *ACM MM*, 2018, pp. 2023–2031.
- [26] D. Chang, K. Pang, Y. Zheng, Z. Ma, Y.-Z. Song, and J. Guo, "Your 'flaming' is my 'bird': Fine-grained, or not," in *CVPR*, 2021, pp. 11 476–11 485.
- [27] A. D. Gordon, "A review of hierarchical classification," *Journal of the Royal Statistical Society: Series A (General)*, vol. 150, no. 2, pp. 119–137, 1987.
- [28] A.-M. Tousch, S. Herbin, and J.-Y. Audibert, "Semantic hierarchies for image annotation: A survey," *PR*, vol. 45, no. 1, pp. 333–345, 2012.
- [29] C. N. Silla and A. A. Freitas, "A survey of hierarchical classification across different application domains," *Data Mining and Knowledge Discovery*, vol. 22, no. 1, pp. 31–72, 2011.
- [30] D. D. Lewis, Y. Yang, T. Russell-Rose, and F. Li, "Rcv1: A new benchmark collection for text categorization research," *Journal of machine learning research*, vol. 5, no. Apr, pp. 361–397, 2004.
- [31] A. Mayne and R. Perry, "Hierarchically classifying documents with multiple labels," in *2009 IEEE symposium on computational intelligence and data mining*. IEEE, 2009, pp. 133–139.
- [32] J. Rousu, C. Saunders, S. Szedmak, and J. Shawe-Taylor, "Kernel-based learning of hierarchical multilabel classification models," *Journal of Machine Learning Research*, vol. 7, pp. 1601–1626, 2006.
- [33] A. Esteva, B. Kuprel, R. A. Novoa, J. Ko, S. M. Swetter, H. M. Blau, and S. Thrun, "Dermatologist-level classification of skin cancer with deep neural networks," *nature*, vol. 542, no. 7639, pp. 115–118, 2017.
- [34] Z. Yu, T. Nguyen, Y. Gal, L. Ju, S. S. Chandra, L. Zhang, P. Bonnington, V. Mar, Z. Wang, and Z. Ge, "Skin lesion recognition with class-hierarchy regularized hyperbolic embeddings," in *International Conference on Medical Image Computing and Computer-Assisted Intervention*. Springer, 2022, pp. 594–603.
- [35] J. Yang, M. Gao, K. Kuang, B. Ni, Y. She, D. Xie, and C. Chen, "Hierarchical classification of pulmonary lesions: a large-scale radio-pathomics study," in *Medical Image Computing and Computer Assisted Intervention–MICCAI 2020: 23rd International Conference, Lima, Peru, October 4–8, 2020, Proceedings, Part VI* 23. Springer, 2020, pp. 497–507.
- [36] G. Griffin and P. Perona, "Learning and using taxonomies for fast visual categorization," in *CVPR*, 2008, pp. 1–8.
- [37] S. Bengio, J. Weston, and D. Grangier, "Label embedding trees for large multi-class tasks," in *NeurIPS*, 2010, pp. 163–171.
- [38] T. Gao and D. Koller, "Discriminative learning of relaxed hierarchy for large-scale visual recognition," in *ICCV*, 2011, pp. 2072–2079.
- [39] J. Deng, S. Satheesh, A. C. Berg, and F.-F. Li, "Fast and balanced: Efficient label tree learning for large scale object recognition." in *NeurIPS*, vol. 24, 2011, pp. 567–575.
- [40] R. Cerri, R. C. Barros, A. C. PLF de Carvalho, and Y. Jin, "Reduction strategies for hierarchical multi-label classification in protein function prediction," *BMC bioinformatics*, vol. 17, no. 1, pp. 1–24, 2016.
- [41] J. Chen, P. Wang, J. Liu, and Y. Qian, "Label relation graphs enhanced hierarchical residual network for hierarchical multi-granularity classification," in *Proceedings of the IEEE/CVF Conference on Computer Vision and Pattern Recognition*, 2022, pp. 4858–4867.
- [42] N. Verma, D. Mahajan, S. Sellamanickam, and V. Nair, "Learning hierarchical similarity metrics," in *CVPR*, 2012, pp. 2280–2287.
- [43] N. Srivastava and R. Salakhutdinov, "Discriminative transfer learning with tree-based priors," in *NeurIPS*, 2013, pp. 2094–2102.
- [44] E. Giunchiglia and T. Lukasiewicz, "Coherent hierarchical multi-label classification networks," *NeurIPS*, vol. 33, pp. 9662–9673, 2020.
- [45] A. Dhall, A. Makarova, O. Ganea, D. Pavllo, M. Greeff, and A. Krause, "Hierarchical image classification using entailment cone embeddings," in *Conference on Computer Vision and Pattern Recognition Workshops*, 2020, pp. 836–837.
- [46] J. Chorowski and N. Jaitly, "Towards better decoding and language model integration in sequence to sequence models," *arXiv preprint arXiv:1612.02695*, 2016.
- [47] B. Guo, S. Han, X. Han, H. Huang, and T. Lu, "Label confusion learning to enhance text classification models," in *AAAI*, vol. 35, no. 14, 2021, pp. 12 929–12 936.
- [48] C. Wah, S. Branson, P. Welinder, P. Perona, and S. Belongie, "The caltech-ucsd birds-200-2011 dataset," 2011.
- [49] S. Maji, E. Rahtu, J. Kannala, M. Blaschko, and A. Vedaldi, "Fine-grained visual classification of aircraft," *arXiv preprint arXiv:1306.5151*, 2013.
- [50] J. Krause, M. Stark, J. Deng, and L. Fei-Fei, "3D object representations for fine-grained categorization," in *International Conference on Computer Vision Workshops*, 2013, pp. 554–561.
- [51] J. Wehrmann, R. Cerri, and R. Barros, "Hierarchical multi-label classification networks," in *ICML*. PMLR, 2018, pp. 5075–5084.
- [52] A. Paszke, S. Gross, F. Massa, A. Lerer, J. Bradbury, G. Chanan, T. Killeen, Z. Lin, N. Gimelshein, L. Antiga *et al.*, "Pytorch: An imperative style, high-performance deep learning library," *NeurIPS*, vol. 32, pp. 8026–8037, 2019.
- [53] J. Deng, W. Dong, R. Socher, L.-J. Li, K. Li, and L. Fei-Fei, "ImageNet: A large-scale hierarchical image database," in *CVPR*, 2009, pp. 248–255.
- [54] R. R. Selvaraju, M. Cogswell, A. Das, R. Vedantam, D. Parikh, and D. Batra, "Grad-cam: Visual explanations from deep networks via gradient-based localization," in *CVPR*, 2017, pp. 618–626.
- [55] A. Li, T. Luo, Z. Lu, T. Xiang, and L. Wang, "Large-scale few-shot learning: Knowledge transfer with class hierarchy," in *Proceedings of the IEEE/CVF conference on computer vision and pattern recognition*, 2019, pp. 7212–7220.
- [56] T. Mikolov, I. Sutskever, K. Chen, G. S. Corrado, and J. Dean, "Distributed representations of words and phrases and their compositionality," *Advances in neural information processing systems*, vol. 26, 2013.
- [57] B. Hariharan and R. Girshick, "Low-shot visual recognition by shrinking and hallucinating features," in *Proceedings of the IEEE international conference on computer vision*, 2017, pp. 3018–3027.
- [58] S. Qiao, C. Liu, W. Shen, and A. L. Yuille, "Few-shot image recognition by predicting parameters from activations," in *Proceedings of the IEEE conference on computer vision and pattern recognition*, 2018, pp. 7229–7238.
- [59] M. Douze, A. Szlam, B. Hariharan, and H. Jégou, "Low-shot learning with large-scale diffusion," in *Proceedings of the IEEE conference on computer vision and pattern recognition*, 2018, pp. 3349–3358.
- [60] C. Barata, J. S. Marques, and M. Emre Celebi, "Deep attention model for the hierarchical diagnosis of skin lesions," in *Proceedings of the IEEE/CVF Conference on Computer Vision and Pattern Recognition Workshops*, 2019, pp. 0–0.
- [61] P. Tschandl, C. Rosendahl, and H. Kittler, "The ham10000 dataset, a large collection of multi-source dermatoscopic images of common pigmented skin lesions," *Scientific data*, vol. 5, no. 1, pp. 1–9, 2018.
- [62] G. Argenziano, H. Soyer, V. De Giorgi, D. Piccolo, P. Carli, M. Delfino *et al.*, "Interactive atlas of dermoscopy," *EDRA Medical Publishing & New Media*, pp. 1,2,5, 2000.